Aerodynamic Analysis for the Mathematical Model of a Dual-System UAV

Yael F. López-Briones
Escuela Superior de Ingeniería
Mecánica y Eléctrica-IPN
México City, MÉXICO
ylopezb1400@egresado.ipn.mx

Luz M. Sánchez-Rivera
UMI-LAFMIA
CINVESTAV
México City, MÉXICO
luz.maria.sanchez@cinvestav.mx

Alfredo Arias-Montano
Escuela Superior de Ingeniería
Mecánica y Eléctrica-IPN
México City, MÉXICO
aarias@ipn.mx

Abstract—In this paper, we present the use of reverse-engineering like techniques to analyse the proposal of a Dual-System Unmanned Aerial Vehicle. Such vehicles are capable of performing vertical flight with the use of a multi-rotor system and then transition into horizontal flight without modifying their structure. The main features and dimensions are captured. A prototype was built and then modeled using Computer-Aided Design (CAD) software. Aerodynamic characteristics for the model were obtained using accurate computational analysis tools, namely XFLR5, Xfoil and ANSYS Fluent®. Simulation results for the airfoil, the wing and the complete airframe are presented and compared. Results were studied and adapted for the longitudinal model of the UAV by means of the stability derivatives. The study serves as good basis to implement the aerodynamic data in the mathematical model of the platform and perform future control simulations. Besides, it lays the foundation for future research and improvement on the knowledge of the characteristics and capabilities of this type of aircraft.

Index Terms—Dual-System UAV, Fixed-Wing VTOL, Hybrid UAV, Aerodynamic Study, Multi Rotor

I. INTRODUCTION

Unmanned Aerial Vehicles (UAVs) have been widely used worldwide to perform diverse tasks which would be otherwise impossible for conventional aircraft. Nowadays, their use extents not only to military, defence or reconnaissance applications, but to civil operations, such as transport, agriculture or photography.

In general, UAVs' configuration can be classified as either Fixed-Wing or rotorcraft. Whereas Fixed-Wing vehicles perform better during horizontal flight and have remarkable advantages regarding cruising speed, flight range or endurance over rotorcraft vehicles, they usually lack simplicity for takeoff and landing, requiring large runways or especial equipment, not to mention the wide space they need in order to maneuver in cruise flight. Here is where the rotorcraft UAVs play a very important role in ensuring the safety and reliability for the vehicle during takeoff and landing, as well as other mission stages where hovering is preferred to cruise flight.

Clearly, both configurations have very specific characteristics depending on the application. However, it is possible to combine them in a single platform, a task that has been attempted over the last decade by means of hybrid vehicles. These integrate the flight advantages of Fixed-Wing and rotorcraft aeroplanes.

The type of hybrid vehicle addressed in this paper is known as Dual-System, which make use of a multi-rotor system for vertical operation and a pusher/puller rotor for cruise flight [1]. This concept aircraft stands out for its stability and simplified mechanical design, giving the aircraft reliability and simplicity. Furthermore, it requires little maintenance and, if the aircraft characteristics were to be studied, the analysis for each flight phase could be performed in a separate manner. Due to its effectiveness, many platforms of this kind have been designed and some others, initially being Fixed-Wing models, were adapted for its use as a Dual-System [2].

Development of Dual-System vehicles and of UAVs in general encompasses various stages. After a mission planning definition and platform configuration is selected, design and weight estimation follows, including selection of on-board equipment. Afterwards, Finite Element Method (FEM), Computational Fluid Dynamics (CFD) or control analyses may follow. Only after an iterative process of redesign based on the results of each stage the final platform is manufactured, and flight tests are conducted. Nonetheless, these steps take a long time and it is not possible to properly cover each one in detail.

Generally speaking, the approach taken in the analysis of Dual-System UAVs has unfortunately led to studies that only cover conceptual design where the final product is never built or studies where even though the platform is manufactured, inaccurate research techniques are used [3]. This in turn could also lead to poor vehicle performance. Another approach is to make use of known theory for adequate sizing but using poor accuracy numerical analysis [4].

In addition to the previous problems, to the best of our knowledge, Dual-System UAVs have not yet been manufactured in Mexico, the platform is instead acquired from foreign developers, as in the case of the Arcturus Jump 20 [1]. As can be seen, insufficient infrastructure obligates the country to expend a considerable amount of resources in what would otherwise be easily affordable technology.

Therefore, the main contribution of this study is to computationally estimate the aerodynamic derivatives for a Dual-System as a mean to use them in the mathematical model and control system design for flight simulation as future work. Although the results of this methodology could be compared

against theoretical or experimental methods, to the best of our knowledge, theory does not cover the complex effects of the flow and the experiments will be included in future research.

The remainder of the paper is organized as follows. Section II presents the development of the Dual-System aircraft and includes the mathematical model of the vehicle. In Section III CFD simulations are undertaken as well as the underlying theory is described. Next, in section IV aerodynamic derivatives are obtained and a discussion of results is given. Finally, in section V, conclusions are presented and future work is established.

II. Aircraft development

A. Airplane Description and Prototype Construction

The prototype was adopted from a commercially available platform due to its proven ease of construction and rigidity once built, the FT Explorer [5]. Nevertheless, the original design has been also adapted as a Vertical Takeoff and Landing (VTOL) platform. Therefore, two beams or motor pods have been added under the wing on each side of the symmetrical plane of the UAV. Each extremity of the pods will carry a motor with its respective propeller, comprising the multi rotor system.
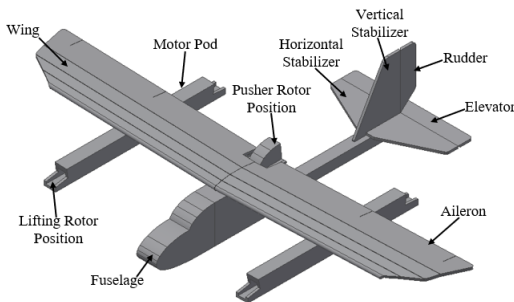

Fig. 1. CAD Design of the Dual-System.

Fig. 1 shows the aircraft modeled using Autodesk® Inventor® Computer-Aided Design (CAD) software. As previously stated, its functioning comprises two systems that are operationally separated. During takeoff, only the multi rotor system is turned on and motion is controlled by the differential thrust from the lifting rotors. Yaw, roll and pitch control is similar to that of a quadrotor. For the transition phase from hovering to horizontal flight, the pusher rotor is used to give forward acceleration and gradually reach the desired cruising speed. This is usually the most crucial phase in all hybrid vehicles, because they present instabilities and the integrity of the aircraft is at risk. However, the Dual-System tends to overcome this problem thanks to the geometry of the platform. In particular, the wing aids in the process of keeping the aircraft airborne. Finally, during cruise flight the multi-rotor system is no longer needed and lifting rotors can be turned off. Control is achieved by the push motor and control surfaces such as ailerons, elevators and rudders [3].

The selected multi-rotor configuration is known as the "H" or "11" fixation method, where the motor pods are parallel to each other, instead of the "X" method typical in quadrotors. This fixation method has proven to be more efficient [6]. It is less affected by the rotational motion of the propeller and produces less interference in the flow during flight. The wing also has a dihedral angle of 2° as a mean for providing lateral static stability [7].

Airplane manufacture was started. The main material used for construction is cardboard foam, which is practically inexpensive and easily acquired. Besides, manipulation is simple and it gives flexibility in case more changes were needed. An image for the fuselage structure is presented in Fig. 2a., whereas Fig. 2b. shows an image of the wing.
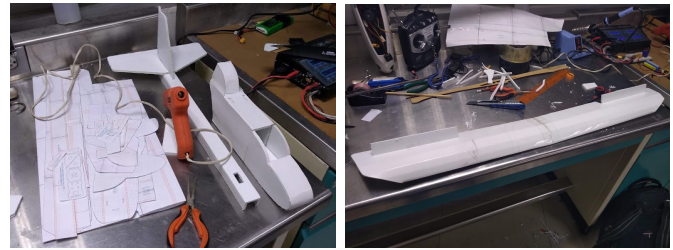
(a) Fuselage structure. (b) Wing structure.

Fig. 2. Dual-System UAV Prototype.

Table I lists the principal components for the platform and an initial mass estimation. "Others" comprise additional but lightweight electronics and equipment. As can be seen, the final mass for the prototype will not exceed the usual values for this type of airplane, which are above 1.5 kg.

TABLE I
INITIAL MASS ESTIMATION FOR THE DUAL-SYSTEM

Component	Quantity	Mass (kg)
Airframe	1	0.290
Battery	1	0.288
Lifting Motors	4	0.240
Pusher Motor	1	0.076
Propellers	5	0.030
Others	-	0.200
Total	-	1.124

B. Flight Profile

The flight mission profile is shown in Fig. 3. Takeoff is where the multi rotor system for hovering is firstly used. Besides, during transition from hovering to cruise a little altitude is lost. The mission may include a loiter phase where the aircraft patrols a certain area. Finally, for the next transition, speed is reduced and the mission concludes with a vertical landing.

C. Mathematical Model

The mathematical model shown here is based on the equations presented in [8] and [9], which use the Newton-Euler formulation. Although the previous studies develop a model for a Dual-System, in the former the aerodynamic parameters
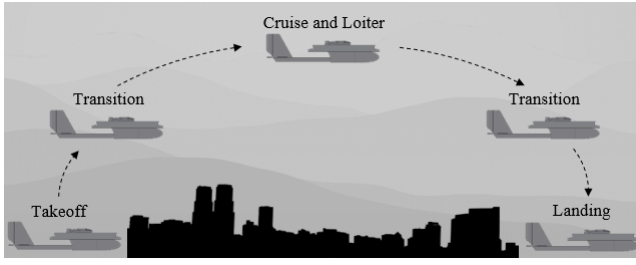
Fig. 3. Flight profile of the vehicle.

were not taken from the original platform and in the latter the objective was control optimization.

If we consider the components of total force acting on a rigid body, given by:

$$\sum \Delta m a_x^\ell = X \; ; \quad \sum \Delta m a_y^\ell = Y \; ; \quad \sum \Delta m a_z^\ell = Z \quad (1)$$

where Δm is the incremental mass at point $p(x; y; z)$ in the rigid body and $a_x^\ell; a_y^\ell; a_z^\ell$ are the components of inertial acceleration. These components are represented as:

$$a_x^\ell = \dot{U} - rV + qW \quad ; \quad a_y^\ell = \dot{V} - pW + rU$$
$$a_z^\ell = \dot{W} - qU + pV \quad (2)$$

In these equations, $p; q$ and r are angular velocity components about the $ox; oy$ and oz axes, respectively. Velocity and acceleration components along the same axes are denoted by $(U; V; W)$ and $(\dot{U}; \dot{V}; \dot{W})$ respectively.

After substitution (2) in (1) and rearranging, the resulting total force components with respect to the body frame are written in matrix form as:

$$\begin{bmatrix} \dot{U} \\ \dot{V} \\ \dot{W} \end{bmatrix} = \begin{bmatrix} rV - qW \\ pW - rU \\ qU - pV \end{bmatrix} + \frac{1}{m} \begin{bmatrix} X \\ Y \\ Z \end{bmatrix} \quad (3)$$

In (3), m is the the total mass of the body and the external forces are:

$$\begin{bmatrix} X & Y & Z \end{bmatrix}^T = F_g + F_a + F_{p;m} + F_{p;p} \quad (4)$$

where F_g is force due to gravitational effects, F_a is force due to aerodynamic effects, $F_{p;m}$ is propulsion force due to the multi-rotor system and $F_{p;p}$ is propulsion force due to the pusher propeller. In this work, the necessary derivatives for the computation of F_a will be obtained through CFD simulations. Even though the aerodynamic effects include those of the rotors, the wing and the fuselage, the wing is the main contributor to the flow characteristics.

III. CFD SIMULATIONS

Forces acting on a solid body immersed in a fluid are due to pressure distribution and shear stress over the body surface [10]. Lift (L) is the force component of the net aerodynamic force, perpendicular to the flow direction, drag (D) is the force component along the flow direction [11]. However, to characterize the flow over a body regardless of its shape, it is convenient to use dimensionless parameters derived from the

above description. For that, the lift C_L, drag C_D and moment C_M coefficients are defined in (5), (6) and (7) as:

$$C_L = \frac{L}{\frac{1}{2} \rho_1 V_1^2 S} \quad (5)$$

$$C_D = \frac{D}{\frac{1}{2} \rho_1 V_1^2 S} \quad (6)$$

$$C_M = \frac{M}{\frac{1}{2} \rho_1 V_1^2 S c} \quad (7)$$

In these equations, ρ_1 and V_1 are the freestream density and velocity, respectively. S is equal to the wing planform area for an aircraft [12] and c is equal to the Mean Aerodynamic Chord (MAC), traditionally used in stability and control studies [7]. In the case of an airfoil, the equations are slightly modified, the coefficients are denoted by lowercase letters (c_l, c_d and c_m) and the reference area $S = c(1) = c$ since forces and moments are per unit span. This is useful, because it makes comparison of the aerodynamic properties between an airfoil and a 3D wing possible.

CFD simulations considered longitudinal symmetric flight. However, propeller wake will not be included in the analysis because the propellers in the motor pods will be powered off and aligned with the flow to improve efficiency in real flight. Flow conditions were established and geometric dimensions were measured directly from the airplane, both appear in Table II. Aspect Ratio (AR) is the ratio between the wing span (b) and the MAC. The Reynolds Number (Re) is an important parameter that represents either the smooth and regular (laminar) or random (turbulent) nature of the flow [10].

TABLE II
RELEVANT PARAMETERS FOR ANALYSIS

Wing Span (*b*)	MAC	Wing Area (*S*)	*AR*
0.955 m	0.1211 m	0.0997 m²	9.15
Viscosity ( )	**Cruise Speed (*V*)**	**Density ( )**	***Re***
1.7894e-5 kg/m-s	25 m/s	1.225 kg/m³	0.216e⁶

To study the aerodynamic properties of the prototype, three different software packages were used. For every one of them, the selected speed was $V = 25\ m=s$ because it is within the typical cruising speed value for an UAV. In addition to that, the selected range of angles of attack is from $\alpha = -20^o$ to $\alpha = 20^o$. This range is used because, even though 2D software data predictions are considered valid just beyond maximum lift coefficient, an appropriate outlining of the drag polar can be made.

Firstly, 2D CFD simulations were performed in the popular XFLR5 and Xfoil programs. Both are oriented to the design and analysis of low Reynolds number airfoils and operate in a similar manner. In the particular case of Xfoil, the software is based on the use of panel methods, which could be reviewed in [10], with Boundary Layer (BL) estimations for viscous analysis. To perform an analysis, the user imports the airfoil geometry and inputs flow data like Reynolds number and angle of attack. For the airfoil selection, the cross section

of the wing was matched to the Wortmann FX 77-W-121 airfoil, in a similar manner to [13]. Based on the average results of the 2D simulations, the airfoil maximum lift coefficient is ($C_{lmax} = 1.3909$) at 10.25^o. The zero-lift angle of attack ($\alpha_{L=0} = -2.7^o$) and maximum lift-to-drag ratio ($C_l/C_d = 75.0019$) at 10°. Calculations considered Standard Sea-Level Conditions (SSL).

Secondly, since a more accurate analysis was crucial, another series of CFD simulations were performed in the high-fidelity ANSYS Fluent® software. The CAD model was further simplified and prepared to reach corvengence in the solution. The complete airframe of the UAV and a straight rectangular wing with no dihedral but with the prototype dimensions were analysed separately. Since no asymmetrical conditions were to be analysed and the UAV is symmetrical along the longitudinal axis only half of the airplane was used, saving computational cost and time. The fluid domain is a rectangle and the quarter-chord point of the wing of the models was placed at the origin. The rectangle extended from -6 m to 34 m in X (platform longitudinal) direction, from -6 m to 6 m in Y direction and from 0 to -6 m in the Z direction. Apart from the main enclosure, an additional rectangle in the vicinity and downstream of the model was added in order to refine the mesh later in Fluent® and accurately capture the characteristics of the wake. The final boundary conditions are a velocity inlet in the front part of the rectangle, a pressure outlet with atmospheric condition at the back, a symmetry plane for the mid-plane of the domain and walls at the remaining surfaces, including those of the UAV and the wing.

The type of flow for our case is turbulent according to the Reynolds number, therefore an appropriate turbulence model should be selected for the analysis. ANSYS® Documentation recommends either the use of the Realizable $k-\epsilon$ or SST $k-\omega$ turbulence models for standard cases [14]. In UAV analysis, boundary layer separation may occur and resolving the viscous sublayer is recommended if affordable, however, the $k-\omega$ models usually require a finer mesh near the wall, otherwise accuracy may be lost. For that reason, the Realizable $k-\epsilon$ model with Standard Wall Treatment will be used.

The Realizable $k-\epsilon$ model is part of the Reynolds Averaged Navier-Stokes Simulation (RANS) based models. Since turbulent flow is considered, the properties of the flow fluctuate over time but not their statistically averaged value and the governing equations are modified through what is called Reynolds-averaging to obtain the RANS equations [14]. At the same time, the $k-\epsilon$ model is a two equation model that includes two additional transport equations to represent the turbulent properties of the flow. k is the turbulent kinetic energy and is a measure of how much energy is contained in the fluctuations, its transport equation is given by (8).

$$\frac{\partial}{\partial t}(\rho k) + \frac{\partial}{\partial x_j}(\rho k u_j) = \frac{\partial}{\partial x_j}\left[\left(\mu + \frac{\mu_t}{\sigma_k}\right)\frac{\partial k}{\partial x_j}\right] + G_k + G_b - \rho\epsilon - Y_M + S_k \quad (8)$$

On the other hand, ϵ is the turbulent dissipation and it is a measure of the rate at which turbulent kinetic energy dissipates, its transport equation is given by (9).

$$\frac{\partial}{\partial t}(\rho\epsilon) + \frac{\partial}{\partial x_j}(\rho\epsilon u_j) = \frac{\partial}{\partial x_j}\left[\left(\mu + \frac{\mu_t}{\sigma_\epsilon}\right)\frac{\partial \epsilon}{\partial x_j}\right] + \rho C_1 S\epsilon - \rho C_2 \frac{\epsilon^2}{k + \sqrt{\nu\epsilon}} + C_{1\epsilon}\frac{\epsilon}{k}C_{3\epsilon}G_b + S_\epsilon \quad (9)$$

The previous equations are already embedded in the software and there is no need to modify them. Essentially, if k is higher there will be more fluctuations and the contrary is true for ϵ, the higher its value the fewer fluctuations. It is important to have in mind that these quantities are based on experimental results and are not known beforehand, therefore, the default values of the solver will be used.

Taking everything into account, mesh generation took place. For that, a Poly-Hexcore mesh that took advantage of ANSYS® mosaic meshing technology was used instead of the traditional tetrahedral mesh. This is also practical because it produces a high quality mesh with less computational power. Besides, the Realizable $k-\epsilon$ model requires the first cell of the mesh to be located at a y^+ value of approximately 1 and a growth rate no higher than 1.2. A grid independence study was performed, and finally, a mesh consisting of 1.5 million elements with a maximum skewness value of 0.92 and a minimum orthogonal quality of 0.08 was achieved on average for all simulations. These values ensure that the quality of the mesh is sufficient for the accuracy needed.

For the solution, since flow is incompressible, the steady and pressure-based Fluent® solver settings were selected. The only modified reference values for post-processing were the reference area ($A = 0.049851\ m^2$) and velocity, which corresponds to cruising speed. The reference length did not have to be modified thanks to the location of the origin. The scheme chosen for the solution was the Semi-Implicit Method for Pressure Linked Equations (SIMPLE) to save computational power. However, discretization was of second order and the gradient setting was Least Squares Cell Based. To monitor solution convergence, residuals of continuity, velocity, k and e required to be less than $1e^{-03}$. Even though convergence criteria is established, it is important to monitor additional physical quantities to confirm that they converge to a certain value, only after that it can be said that a final and accurate solution was reached. For that, monitors of the aerodynamic coefficients and mass balance were verified. In those cases were the solution fluctuated, the Under-Relaxation Factors helped to reach a slow but stable solution [14].

Fig. 4 shows the lift coefficient versus angle of attack comparison for all numerical simulations. As may be observed, the slope is very similar and the graphs are homogeneous for the four cases. Besides, both the XFLR5 and the Xfoil predictions are very close to each other, as expected. Nonetheless, it should be remembered that just above stall these values are not precise anymore. For both 2D programs a little increment in lift is observed after stall, which in reality is not true. Instead the UAV has a gentle stall because a turbulent boundary layer has more resistance to flow separation, as it is easily observed in the 3D graphs. Another remark is that the maximum lift

coefficient is highest for the airfoil, reduces for the wing and is minimum for the complete airframe.
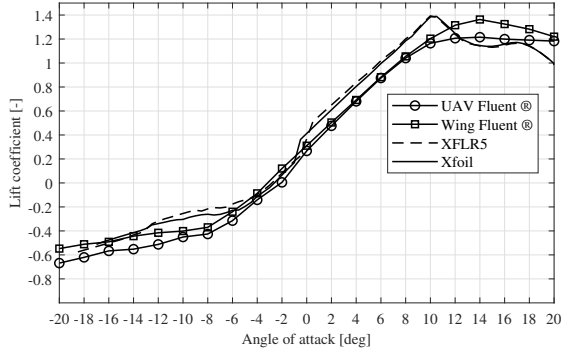

Fig. 4. Lift coefficient versus angle of attack.

Fig. 5 presents the drag coefficient versus angle of attack comparison for all numerical simulations. Again, the values of the airfoil curves match accordingly. There seems to be a certain "*drag bucket*" in the curve for values from 10° to 11°, but this behaviour only appears at certain laminar flows, after this region, the slope increases again. There also appears a substantial increase in drag for the three-dimensional cases, this is mainly due to the fuselage because it has not been optimised.
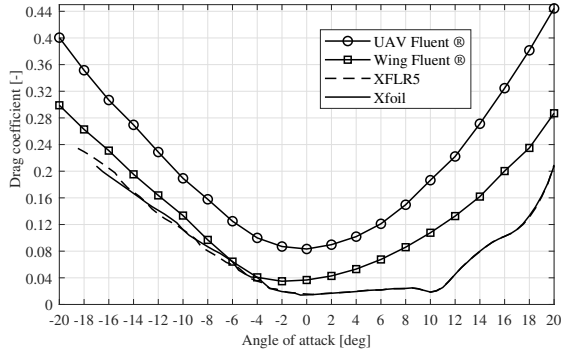

Fig. 5. Drag coefficient versus angle of attack.

In Fig. 6 the moment coefficient versus angle of attack is presented. The airfoils present longitudinal static stability because the slope is negative and the pitching moment would be restoring [7]. In the case of the wing and the airframe, the slope is positive, this may be due to the fact that neither the selected airfoil nor the fuselage geometry are appropriate for turbulent flow. To compensate for this instability, the components of the airplane could be easily changed so that the center of gravity lies in a position that overcomes the non-restoring pitching moment.

The pressure variation over the surface with flow-paths at 14°, where maximum lift coefficient was achieved, is presented in Fig. 7a. Sanity checks were done and it was verified that the pressure was higher at the lower surface,
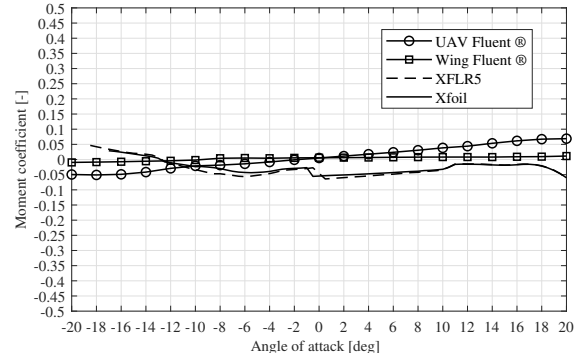

Fig. 6. Moment coefficient versus angle of attack.

which indicates a resultant lift force. Meanwhile, Fig. 7b shows flow-paths near the wing tips, where tip vortices and consequently more induced drag are being generated. Induced drag is an unfavorable three-dimensional effect [10], an effect that could be reduced by adding winglets on the airplane. The effect of the motor pods in the structure is also noticeable, when the flow collides with them several disturbance and more drag is being generated. Since the prototype concept was directly modeled with no changes in geometry future work may include adding winglets and observing the flow-paths again.
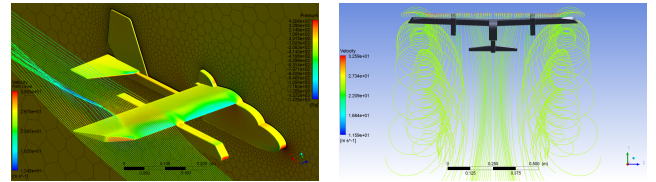
(a) Pressure Contours on the surface   (b) Wing tip vortices of the flow.
of the UAV.

Fig. 7. Pressure Contours and Flow-Path Lines (Re = 0.216e^6,   = 14°).

Lastly, Fig. 8a shows the pressure contours at an XY plane located at Z = -0.37 m and it is compared with Fig. 8b which shows velocity vectors at the same location. At this location the boundary layer thickness has increased considerably. In fact, further to the wing tips there exists reversal of the flow, a consequence of flow separation. This is also a consequence of the high angle of attack, at this point flow has separated from the surface and the airplane has begun to stall.

IV. LONGITUDINAL DERIVATIVES AND RESULTS

The estimation of the longitudinal stability derivatives developed here is based on [7]. Since flow is incompressible, dependency of the aerodynamic coefficients on speed is insignificant and the corresponding terms are omitted. First, the axial force due to axial velocity, normal velocity, pitch rate, rate of change of normal velocity and elevator are:

$$X_u = \quad 2C_D \; ; \; X_w = C_L \quad \frac{dC_D}{d}$$
$$X_q = 0 \; ; \; X_{\dot{w}} = 0 \; ; \; X = 0 \tag{10}$$